Mathematical Biosciences and Engineering

https://www.aimspress.com/journal/mbe

MBE, 23(11): 3320–3347.
DOI: 10.3934/mbe.2026114
Received: 21 January 2026
Revised: 05 August 2026
Accepted: 11 September 2026
Published: 06 November 2026

Research article

State-space modeling and estimation for motility assay experiments

John Stockton[1,2,*] **and John Fricks**[1]

[1] School of Mathematics and Statistical Sciences, Arizona State University, Tempe, AZ 85281, USA
[2] School of Mathematics and Natural Sciences, Arizona State University, New College of Interdisciplinary Arts and Sciences, 4701 W Thunderbird Rd, Glendale, AZ 85306, USA

* **Correspondence:** Email: john.stockton@asu.edu.

Abstract: Microtubule gliding assays have been an important experimental tool for investigating intracellular molecular motor transport systems. A statistical method to estimate the parameters of a stochastic model describing the movement of a microtubule in a kinesin-microtubule gliding assay experiment is presented. Two models are proposed: the first is an approximate discretization and modification of an existing system of stochastic differential equations describing microtubule motion proposed by Gibbons et al. (2001), and a second version accommodates some behaviors encountered in motility assay experiments, such as curvature and pausing. To aid in understanding the relationship between kinesin motors and microtubules, the model describes metrics such as the velocity of a microtubule in a gliding assay experiment, the effect on the velocity based on the amount of curvature in the microtubule, and how frequently a microtubule may pause its movement. Parameter estimation for the models will employ a stochastic expectation-maximization (EM) algorithm with the expectation step approximated by particle filtering techniques.

Keywords: microtubule gliding assays; stochastic differential equations; state-space models; particle filtering; stochastic EM algorithm

1. Introduction

Molecular motors are a class of proteins which convert chemical energy to mechanical energy and often act as a transport mechanism for organelles and various cargo within eukaryotic cells. Since the discovery of the kinesin family of molecular motor proteins in eukaryotic cells as structurally distinct from from myosin and dynein motors in the 1980s [1], extensive research has been conducted over their interaction with microtubules, a class of cytoskeletal polymers formed by tubulin proteins as a hollow tube that act as the primary track upon which molecular motors attach, such as the discovery of the remarkable processivity of kinesin motors to remain bound to a microtubule [2] and the discovery

that microtubules do not act simply as a passive platform for kinesin motors to attach and transport cargo, but are instead an active mechanical communicator with molecular motors [3]. By the late 1980s, advancements in imaging technology allowed for better understanding of binding sites between microtubules and molecular motors such as kinesin using electron microscopy [4]. The model for kinesin movement within eukaryotic cells remains that they move using their heads in a "walking" fashion [5]. As a result of an innate polarity of the microtubule and the molecular motor type, kinesin motors are only able to attach to the "plus end" orientation of a microtubule which often leads to the periphery of the cell; in contrast, dynein motors attach in a "minus end" orientation of a microtubule, typically leading in the direction of the nucleus of the cell [6].

One particular type of experiment used to study the relationship dynamics of kinesin motors and microtubules, known as a microtubule gliding assay experiment, consists of coating a substrate with kinesin motors where the tails are attached to the substrate and the heads facing outward, then stabilized microtubules are placed on the slide and the motion of each microtubule is tracked as it interacts with the heads of the kinesin [2, 7] with the minus end of the microtubule as the leading point of its transit. Experiments of this type have been commonly designed to answer questions regarding how the density of kinesin motors affects microtubule movement [2, 8], the forces governing the attachment and detachment of kinesin motors to a microtubule [9], or even about the effect of the substrate upon which the kinesin are adsorbed [10, 11].

The purpose of this paper is to present a stochastic time series model and to carry out statistical inference to explain the movement and behavior of the microtubule across a substrate covered by kinesin motors and to link that behavior to experimental data. Here, a time series model will be derived, which is based on a system of stochastic differential equations to describe microtubule movement in [12]. To the best of our knowledge at the time of writing, data from gliding assay experiments have not previously been applied to a study with a primary focus on implementing statistical methods of time series analysis.

We will demonstrate two closely related models, both of which can be fit into a hidden Markov model framework where a hidden state tracks the state variables that are the predicted coordinates of a midpoint between the endpoints of a microtubule and an angle describing the direction of travel for the microtubule across a planar surface. Depending on which of the two proposed models is used, the observation variables represent the specific points on the microtubule that are convenient for experimentalists to track, including, but not limited to, the endpoints of the microtubule. The first and simpler model, derived directly from the system of stochastic differential equations from [12], includes only these aforementioned state and observation variables and may still be used here to perform statistical inference regarding the parameters for the average velocity and variance components for each of the state variables and coefficients related to the noise of the observations. As a result of limitations of the simplified model proposed in [12], both versions of our model include accommodations for the following behaviors in empirical data. The first and simpler version of our model includes measures to reflect potential pauses in the movement of the microtubule possibly caused by kinesin motors failing to attach or detach from the microtubule. The second model is an extension of the first model inspired by attributes from experimental data, which accommodates inferences regarding any curvature of the observed microtubule.

This paper is outlined as follows. In Section 2, the state-space models are defined and detailed in full. With parameter estimation from these state-space models being an ultimate goal, Section 3

details the particle filter and stochastic expectation-maximization (EM) algorithm used to numerically calculate parameter estimators. Section 4 examines the results of parameter estimation for the proposed methods from simulated microtubule gliding assay experiments as well as for real experimental data using a glass surface substrate.

2. Stochastic models for gliding assays

In this section, we will present stochastic models for gliding assays that include relevant parameters that will form the basis for the estimation procedures in subsequent chapters. The statistical procedures will rely on creating a state-space model consisting of a state model, typically describing the dynamics of the system under study, and an observational model, which typically models observational error added to the underlying dynamics. The state equations will be denoted by the vector-valued function $\mathbf{X}$ on t, with t representing time. Specifically, the system at the current time is represented by a function $\mathbf{g}$ as a function of the state variables at the previous time point along with stochastic perturbations defined below. The observation equations are designed to account for the stochastic error for the actual data which represents the location of the endpoints of a microtubule at any given time based on the predicted location attained by the state equations. Hence, the system of equations for the observation variables is defined by the function $\mathbf{Y}(t)$ which is itself a function of the current state $\mathbf{X}(t)$ along with stochastic terms independent of those in the state model.

In the first model, the state equations include variables consistent with those in [12] of the rectangular coordinates of the midpoint between the endpoints of the microtubule, denoted as (M^x, M^y), measured in their distance from an origin, and by the central angle, denoted by θ, with the terminal side formed by the line segment adjoining the midpoint with the minus end of the microtubule (the leading point in the travel direction of the microtubule). Hence, the state variables in the first proposed model can be denoted by the following vector:

$$\mathbf{X}(t)' = (M^x(t), M^y(t), \theta(t)).$$

The precise notation of the original system of stochastic differential equations as proposed in [12] is as follows, with modifications only to represent the rectangular coordinates of the midpoint of the microtubule as previously introduced in $(M^x(t), M^y(t))$; also, $W_{\{\cdot\}}(t)$ has replaced the notation to represent independent Brownian motions in their respective components.

$$dM^x(t) = \frac{1}{\zeta_{\parallel}}[F_{\parallel}dt + dW_{\parallel}(t)]\cos(\theta(t)) - \frac{1}{\zeta_{\perp}}[F_{\perp}dt + dW_{\perp}(t)]\sin(\theta(t)),$$

$$dM^y(t) = \frac{1}{\zeta_{\parallel}}[F_{\parallel}dt + dW_{\parallel}(t)]\sin(\theta(t)) + \frac{1}{\zeta_{\perp}}[F_{\perp}dt + dW_{\perp}(t)]\cos(\theta(t)),$$

$$d\theta(t) = \frac{1}{\zeta_{\theta}}[\tau dt + dW_{\theta}(t)].$$

These equations represent a microtubule that is assumed to be rigid, moving along the glass slide represented by a two-dimensional plane. The parameters $F_{\parallel}$ and $F_{\perp}$ represent component forces exerted in the parallel and perpendicular directions, respectively, while in transit in the direction that a

microtubule is traveling; τ represents the torque of the microtubule. The parameters $\zeta_{\|}$ and $\zeta_{\perp}$ refer to the respective friction constants in the parallel and perpendicular direction while ζ_{θ} is referred to as the rotational friction coefficient, which must jointly satisfy the Einstein relations $\zeta_i = k_B T/D_i$ where k_B represents the Boltzmann constant, T represents temperature, and D_i represents the diffusion coefficient (where i acts as a stand-in in for the parallel movement "$\|$", the perpendicular movement "$\perp$", or the rotational movement "θ"). The stochastic processes $W_{\|}$, $W_{\perp}$, W_{θ} are independent, standard Wiener processes representing the Gaussian Langevin forces of their respective state variables.

For convenience, define $\mu_{\|} \equiv \frac{F_{\|}}{\zeta_{\|}}$ and $\mu_{\perp} \equiv \frac{F_{\perp}}{\zeta_{\perp}}$ that will represent component velocities, as well as $\sigma_{\|} \equiv \frac{1}{\zeta_{\|}}$ and $\sigma_{\perp} \equiv \frac{1}{\zeta_{\perp}}$ that will represent component diffusion coefficients. Starting with the stochastic differential equation for the coordinates of the midpoint of the microtubule,

$$dM^x(t) = (\mu_{\|}dt + \sigma_{\|}dW_{\|}(t))\cos(\theta(t)) - (\mu_{\perp}dt + \sigma_{\perp}dW_{\perp}(t))\sin(\theta(t)),$$

$$dM^y(t) = (\mu_{\|}dt + \sigma_{\|}dW_{\|}(t))\sin(\theta(t)) + (\mu_{\perp}dt + \sigma_{\perp}dW_{\perp}(t))\cos(\theta(t)).$$

To be compatible with experimental data that are tracked in uniform increments of time, we will need to form a discrete-time approximation of the system to be compatible with the discrete-time observations. Using the Euler-Maruyama method for the stochastic differential equation for the horizontal coordinate M^x and vertical coordinate M^y, we replace the dt in the first and third terms with Δ, which will represent the time between each observation. In the second and fourth terms, the factors $dW_{\|}(t)$ and $dW_{\perp}(t)$, can also be approximated in discrete-time.

$$\begin{aligned} M^x(t+\Delta) - M^x(t) \approx &\Big(\mu_{\|}\Delta + \sigma_{\|}(W_{\|}(t+\Delta) - W_{\|}(t))\Big)\cos(\theta_t) \\ &- \Big(\mu_{\perp}\Delta + \sigma_{\perp}(W_{\perp}(t+\Delta) - W_{\perp}(t))\Big)\sin(\theta_t), \end{aligned}$$

$$\begin{aligned} M^y(t+\Delta) - M^y(t) \approx &\Big(\mu_{\|}\Delta + \sigma_{\|}(W_{\|}(t+\Delta) - W_{\|}(t))\Big)\sin(\theta_t) \\ &+ \Big(\mu_{\perp}\Delta + \sigma_{\perp}(W_{\perp}(t+\Delta) - W_{\perp}(t))\Big)\cos(\theta_t). \end{aligned}$$

The increments of a Wiener process $(W_i(t+\Delta) - W_i(t))$ are zero-mean Gaussian random variables with variance equal to Δ and are independent for non-overlapping intervals of time.

Finally, assuming data are observed at integer multiples of Δ, the change from continuous time notation to discrete time notation will be adopted for convenience; i.e.,$\forall\ M_n^x \approx M^x(n\Delta)$ will represent the location of the horizontal coordinate after $n\Delta$ units of time have elapsed.

The model will further assume that there is no velocity in a direction perpendicular to its angle of travel, thus implying that $\mu_{\perp} = 0$; to assume otherwise is to imply that a microtubule is able to drift consistently in a transverse direction, which contradicts the empirical evidence and the assumed direction of forces arising from the kinesin motors. For convenience, the redefinition of $\mu \equiv \mu_{\|}$ will be interpreted as the average speed of the microtubule traveling across a kinesin-covered surface. We arrive at the following updated form of the equation for the first model:

$$M_{n+1}^x \approx M_n^x + \Big(\mu\Delta + \sqrt{\Delta\sigma_{\|}^2}\epsilon_n^{\|}\Big)\cos(\theta_n) - \sqrt{\Delta\sigma_{\perp}^2}\epsilon_n^{\perp}\sin(\theta_n), \tag{2.1}$$

$$M_{n+1}^{y} \approx M_{n}^{y} + \left(\mu\Delta + \sqrt{\Delta\sigma_{\parallel}^{2}}\epsilon_{n}^{\parallel}\right)\sin(\theta_{n}) + \sqrt{\Delta\sigma_{\perp}^{2}}\epsilon_{n}^{\perp}\cos(\theta_{n}) , \tag{2.2}$$

noting that $\epsilon_{n}^{\parallel} \sim \mathcal{N}(0,1)$ and $\epsilon_{n}^{\perp} \sim \mathcal{N}(0,1)$ are mutually independent and identically distributed for all n and between all parallel and perpendicular terms.

As for the equation for the angle of rotation θ, using the same approach as used for equations for the rectangular coordinates, define $\mu_{\theta} \equiv \frac{\tau}{\zeta_{\theta}}$ and $\sigma_{\theta} = \frac{1}{\zeta_{\theta}}$. The updated continuous-time version of the stochastic differential equation for the angle is then

$$d\theta(t) = \mu_{\theta}dt + \sigma_{\theta}dW_{\theta}(t) .$$

Thus, the discrete-time series equation using the Euler-Maruyama method once again will ultimately become

$$\theta_{n} \approx \theta_{n-1} + \mu_{\theta}\Delta + \sqrt{\Delta\sigma_{\theta}^{2}}\epsilon_{n}^{\theta} ,$$

where $\epsilon_{n}^{\theta} \sim \mathcal{N}(0,1)$, independent from the other stochastic ϵ terms above for all n, and the redefinitions of μ_{θ} and σ_{θ} are made to compare to Eqs (2.1) and (2.2). Another assumption of this model will be that there is no rotational velocity in any particular direction, so that $\mu_{\theta} = 0$; to assume otherwise is to suggest that the microtubule has consistent clockwise or counterclockwise rotation, which contradicts the empirical evidence. This leads to the final equation for θ:

$$\theta_{n} \approx \theta_{n-1} + \sqrt{\Delta\sigma_{\theta}^{2}}\epsilon_{n}^{\theta} . \tag{2.3}$$

Equations (2.1)–(2.3) would complete the discretizations of the first model as originally proposed in [12]. However, our first and simpler proposed model will include accommodating empirical instances in gliding assay experiments where the microtubule appears to cease its motion for a short period of time, likely representing a prolonged attachment between a kinesin motor and most likely one or both endpoints of the microtubule [10]. In such instances, the microtubule appears to jitter in place; thus, the only parameter of the model that is affected by the microtubule entering a pausing state is the average speed μ, which affects the forward movement of the microtubule in its respective direction. Consequently, a two-state Markov chain, denoted by J_n, will be used as follows. If $J_n = 0$, the microtubule is considered to not be in a paused state while $J_n = 1$ considers the microtubule to be stuck in a paused state. This introduces two more parameters to the state equations: the probability that the microtubule changes from an unpaused state to a paused state, denoted γ_{01}, and the probability that the microtubule changes from a paused state to an unpaused state, denoted γ_{10}. For purposes of maximum likelihood estimation in the sections to follow, we denote the probability of continuing transit, i.e., remaining in an unpaused state, as $\gamma_{00} = 1 - \gamma_{01}$, and the probability of remaining in a paused state between successive observations is $\gamma_{11} = 1 - \gamma_{10}$. Ultimately, this yields the final form of the state equations for the simpler of the two models proposed in this section to include (2.3) and the following:

$$\begin{aligned} M_{n}^{x} &= M_{n-1}^{x} + \left(\mu I_{\{J_{n-1}=0\}}\Delta + \epsilon_{n}^{\parallel}\sqrt{\Delta\sigma_{\parallel}^{2}}\right)\cos(\theta_{n-1}) - \epsilon_{n}^{\perp}\sqrt{\Delta\sigma_{\perp}^{2}}\sin(\theta_{n-1}) , \\ M_{n}^{y} &= M_{n-1}^{y} + \left(\mu I_{\{J_{n-1}=0\}}\Delta + \epsilon_{n}^{\parallel}\sqrt{\Delta\sigma_{\parallel}^{2}}\right)\sin(\theta_{n-1}) + \epsilon_{n}^{\perp}\sqrt{\Delta\sigma_{\perp}^{2}}\cos(\theta_{n-1}) , \end{aligned} \tag{2.4}$$

where $I_{\{\cdot\}}$ represents an indicator function.

The observation equations consider the predicted coordinates of the endpoints of the microtubule, again based currently on the assumption of a rigid structure. These are denoted herein with (U^x, U^y) as the endpoint that is considered the leading point in the direction that the microtubule is traveling, and (L^x, L^y) is the endpoint opposite the leading endpoint. Thus, for some fixed d representing the half-length of the microtubule, the observation equations are then the following.

$$\begin{aligned} U_n^x &= M_n^x + d \cdot \cos(\theta_n) + \sigma\epsilon_n^{U^x} , \\ U_n^y &= M_n^y + d \cdot \sin(\theta_n) + \sigma\epsilon_n^{U^y} , \\ L_n^x &= M_n^x - d \cdot \cos(\theta_n) + \sigma\epsilon_n^{L^x} , \\ L_n^y &= M_n^y - d \cdot \sin(\theta_n) + \sigma\epsilon_n^{L^y} , \end{aligned} \tag{2.5}$$

where $\epsilon_n^{U^x}, \epsilon_n^{U^y}, \epsilon_n^{L^x}, \epsilon_n^{L^y} \sim \mathcal{N}(0, 1)$ are independent and identically distributed for all n and $\sigma > 0$ is a common and fixed standard deviation parameter for each term.

The second model considered in this paper is inspired by one major additional aspect involving the inclusion of the centroid of the microtubule with the experimental data provided for this study, whose rectangular coordinates will be denoted (C^x, C^y). Here, the shape of the microtubule is no longer strictly rigid but will be assumed to be able to form a slight arc. To compute the shape of the microtubule at time index n, the additional measurement in the state-space, denoted δ, will be used to measure the distance between the midpoint (M_n^x, M_n^y) and the prediction of the centroid coordinates using the angle perpendicular to θ_n appropriate to which direction the microtubule is considered to flex at index n. Figure 1 below shows a diagram depicting the physical interpretation of the variables of the model.

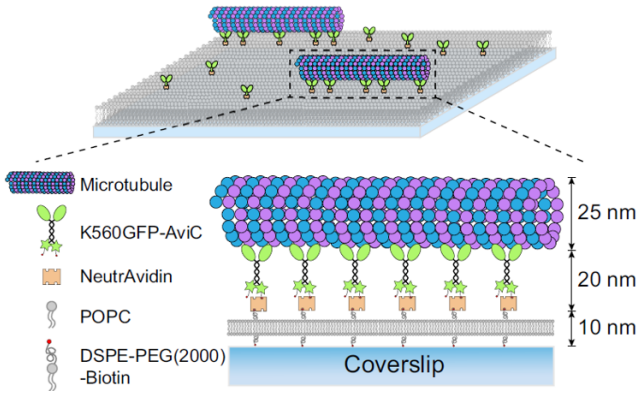


Figure 1. Diagram modeling a microtubule gliding assay experiment on a glass coverslip. K560GFP-AviC refers to biotinylated GFP-labeled *Drosophila* kinesin-1 motors, NeutrAvidin is the link to DSPE-PEG(2000)-Biotin. This diagram depicts a lipid bilayer composed of POPC (1-palmitoyl-2-oleoyl-glycero-3-phosphocholine) that is not present in the experimental data used in this document. (*Image Source*: [11])

In this model, by suggesting that the microtubule has a tendency to straighten, the stochastic differential equation for this model describing the behavior of δ through continuous time is

$$d\delta(t) = -\alpha\delta(t)dt + \sigma_\delta dW_\delta(t) ,$$

where $W_\delta(t)$ is another standard Wiener process that is independent of all previously stated Wiener processes. With a straightforward application of Euler-Maruyama method, this becomes

$$\delta_n = \delta_{n-1} - \alpha\Delta\delta_{n-1} + \epsilon_n^\delta \sqrt{\Delta\sigma_\delta^2}\,, \tag{2.6}$$

where α is the rebounding constant satisfying $0 < \alpha < \frac{1}{\Delta}$ and $\epsilon_n^\delta \sim \mathcal{N}(0,1)$ is independent and identically distributed for all n and all other ϵ. Ultimately, the state variables for this version of the model will be denoted $\mathbf{X}'_n = (M_n^x, M_n^y, \theta_n, \delta_n)$.

Assuming that the total arc length, denoted by λ, is constant throughout the experiment and having a value of δ_n, the distance from the midpoint and the predicted coordinate of the endpoints, denoted by d_n, can be calculated deterministically. By assuming a parabolic shape for the bend of a microtubule, the distance d_n is the solution to the following equation.

$$\sqrt{4\delta_n^2 + d_n^2} + \frac{d_n^2}{2\delta_n} \ln\left(\frac{2\delta_n + \sqrt{4\delta_n^2 + d_n^2}}{d_n}\right) - \lambda = 0\,.$$

The result yields the new set of observation equations for the coordinates of the endpoints U_n, L_n and the centroid C_n as the following equations:

$$\mathbf{Y}_n \equiv \begin{pmatrix} U_n^x \\ U_n^y \\ L_n^x \\ L_n^y \\ C_n^x \\ C_n^y \end{pmatrix} = \mathbf{f}(M_n^x, M_n^y, \theta_n, \delta_n) + \eta_n \equiv \begin{pmatrix} M_n^x + d_n \cdot \cos(\theta_n) \\ M_n^y + d_n \cdot \sin(\theta_n) \\ M_n^x - d_n \cdot \cos(\theta_n) \\ M_n^y - d_n \cdot \sin(\theta_n) \\ M_n^x + |\delta_n| \cos\left(\theta_n - \frac{\pi}{2}s\right) \\ M_n^y + |\delta_n| \sin\left(\theta_n - \frac{\pi}{2}s\right) \end{pmatrix} + \begin{pmatrix} \sigma\epsilon_n^{U^x} \\ \sigma\epsilon_n^{U^y} \\ \sigma\epsilon_n^{L^x} \\ \sigma\epsilon_n^{L^y} \\ \sigma_c\epsilon_n^{C^x} \\ \sigma_c\epsilon_n^{C^y} \end{pmatrix}, \tag{2.7}$$

where $s = sign(\delta_n)$ and $\epsilon_n^{U^x}, \epsilon_n^{U^y}, \epsilon_n^{L^x}, \epsilon_n^{L^y}, \epsilon_n^{C^x}, \epsilon_n^{C^y} \sim \mathcal{N}(0,1)$ independent and identically distributed from all ϵ terms for all n. The additional parameter of σ_c^2 considers the variance component of the centroid that the model considers to be distinguishable from the endpoint observations' variance components.

Another consideration taken into account in this model is the effect that the bend of the microtubule at a given time has on the speed at which the microtubule travels. Specifically, we assume that the speed at which the microtubule is traveling is some function of the amount of curvature at the given time; since the bend can be measured by δ_n, then the speed at index n, is some function $h(\mu, \delta_n)$. This model will adopt the simple linear function $h(\mu, \delta_n) = \mu - \beta|\delta_n|$ where $\beta > 0$.

As a result, the state equations for the second version of the model include (2.3), (2.6), and the following for the midpoint coordinates of the microtubule.

$$\begin{aligned} M_n^x &= M_{n-1}^x + \left((\mu - \beta|\delta_n|)I_{\{J_{n-1}=0\}}\Delta + \epsilon_n^{\parallel}\sqrt{\Delta\sigma_{\parallel}^2}\right)\cos(\theta_{n-1}) - \epsilon_n^{\perp}\sqrt{\Delta\sigma_{\perp}^2}\sin(\theta_{n-1})\,, \\ M_n^y &= M_{n-1}^y + \left((\mu - \beta|\delta_n|)I_{\{J_{n-1}=0\}}\Delta + \epsilon_n^{\parallel}\sqrt{\Delta\sigma_{\parallel}^2}\right)\sin(\theta_{n-1}) + \epsilon_n^{\perp}\sqrt{\Delta\sigma_{\perp}^2}\cos(\theta_{n-1})\,. \end{aligned} \tag{2.8}$$

Ultimately, this provides final observation equations consisting of (2.7) which can be written with additive noise:

$$\mathbf{Y}_n = \mathbf{f}(\mathbf{X}_n) + \eta_n,$$

where $\mathbf{Y}_n := (U_n^x, U_n^y, L_n^x, L_n^y, C_n^x, C_n^y)'$ is the vector containing the observed values of the data at index n, $\mathbf{f}$ is a function computing a predicted location of the observations at time n, and $\eta_n' = (\epsilon_n^{U^x}, \epsilon_n^{U^y}, \epsilon_n^{L^x}, \epsilon_n^{L^y}, \epsilon_n^{C^x}, \epsilon_n^{C^y})$ is the vector representing the noise of the observations (for the first model, the function $\mathbf{f}$ excludes any references to the centroid but is otherwise identical). The ultimate state equations consist of the system with (2.8), (2.6), and (2.3) yielding form of a function

$$\mathbf{X}_n = \mathbf{g}(\mathbf{X}_{n-1}, J_{n-1}, \epsilon_n),$$

where $\mathbf{X}_n := (M_n^x, M_n^y, \theta_n, \delta_n)'$ is a vector including each of the hypothetical realizations of the state variables at index n and $\mathbf{g}$ is a function of the previous state $(n-1)$ and any model parameters and a vector denoting all stochastic terms ϵ_n that account for the variance components in the state variables (again, for the first model, the function $\mathbf{g}$ consists only of Eqs (2.4) and (2.3)). The visual diagram of the microtubule with its model notation is shown in Figure 2.

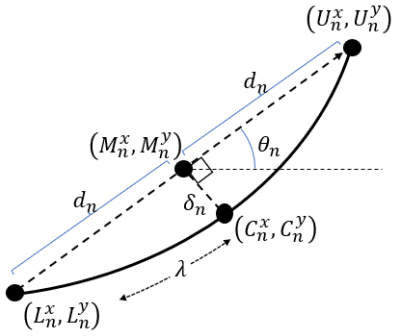


Figure 2. Visual diagram of the microtubule with its model notation. The solid black curve represents the microtubule itself, where λ represents the arc length of the entire microtubule.

It should be noted that there are a few elements in microtubule gliding assay experiments that will not be directly included for the model proposed above and the outcomes of simulated and experimental results. These factors are the result of using a glass surface as the substrate for which the kinesin are attached; thus, the type of surface will currently not be considered. It is well documented that with such a rigid substrate, the velocity of a microtubule is independent of the density of the motors on the surface [8]; for this reason, our models were constructed without the density of the kinesin motors on the glass surface as a factor. Also documented in [12] is that the velocity of a microtubule is independent of the length of the microtubule; consequently, the arc length of a microtubule, represented in the models by λ, will not be considered as a variable in either of the proposed models.

3. Particle filter and EM algorithm

With the models presented in the previous section, we now show a statistical method to estimate the parameters in the state and observation equations. For methods involving maximum likelihood estimation, as with many complex models of dynamics, the full likelihood $L(\Theta|\mathbf{X}_{0:T}, \mathbf{Y}_{0:T})$ is intractable. A nonlinear state-space model such as the proposed model from the previous section requires numerical optimization to find parameter estimators. Specifically, we present a stochastic EM algorithm to handle this task.

Using the second model with state equations comprised of Eqs (2.3), (2.6), and (2.8), the expectation step requires calculating the quantity

$$Q(\Theta|\Theta^{(h)}) = E_{\Theta^{(h)}}[\ell_{\mathbf{X}_{0:N},\mathbf{Y}_{0:N}}(\Theta)|\mathbf{Y}_{0:N}] = \int \ell_{\mathbf{X}_{0:N},\mathbf{Y}_{0:N}}(\Theta)p(\mathbf{x}_{0:N}|\mathbf{Y}_{0:N},\Theta^{(h)})d\mathbf{x}_{0:N}\ , \tag{3.1}$$

where ℓ is the corresponding log-likelihood function if all of the data, both state and observation variables, could be observed and N is the length of the discrete-time series of observations excluding the initial observation $\mathbf{y_0}$, meaning the total length of the time series has a count of $(N+1)$ observations. In the maximization step, (3.1) is maximized across all values of Θ based on the previous value of the vector of parameters $\Theta^{(h)}$, where this maximized value of the vector Θ becomes $\Theta^{(h+1)}$; hence

$$\Theta^{(h+1)} = \underset{\Theta}{\operatorname{argmax}}\, Q(\Theta|\Theta^{(h)}),$$

where the iterative process begins with an initial guess $\Theta^{(0)}$ [13]. The remainder of this section will describe the process of numerically estimating the quantity $Q(\Theta|\Theta^{(h)})$ and obtaining the maximum likelihood estimators for all model parameters. The details presented in this section depict the full model (called the second model in the previous section), which includes all components added to account for perceived curvature in microtubules; the details for the reduced version of the model (called the first model in the previous section) are omitted, yet are similar to what follows.

Let us define $\Theta \equiv (\Theta_{\mathbf{Y}}, \Theta_{\mathbf{X}})$ where $\Theta_{\mathbf{Y}} \equiv (\sigma^2, \sigma_c^2)$ denotes the parameters present in the observation equations of the full version of the model (with an exclusion of σ_c^2 for the reduced version of the model), and $\Theta_{\mathbf{X}} \equiv (\mu, \sigma_{\parallel}^2, \sigma_{\perp}^2, \sigma_{\theta}^2, \sigma_{\delta}^2, \alpha, \beta, \gamma_{01}, \gamma_{10})$ denotes the vector of parameters present in the state equations of the full model (with σ_{δ}^2, α, and β excluded for the reduced version of the model). By recursion and by defining a prior distribution $\mathbf{x}_0 \sim p(\mathbf{x}_0)$, the full-data log-likelihood function becomes the following:

$$\ell_{\mathbf{X}_{0:N},\mathbf{Y}_{0:N}}(\Theta) = \ln[p(\mathbf{X}_0)] + \sum_{n=0}^{N} \ln[p(\mathbf{Y}_n|\mathbf{X}_n,\Theta_{\mathbf{Y}})] + \sum_{n=1}^{N} \ln[p(\mathbf{X}_n|\mathbf{X}_{n-1},\Theta_{\mathbf{X}})]\ . \tag{3.2}$$

Note that in Eq (3.1), we also require the distribution $p(\mathbf{x}_{0:N}|\mathbf{y}_{0:N},\Theta)$, which cannot be expressed in closed form for the models presented in this paper. To approximate this distribution, we adopt a bootstrap particle filter; this method approximates the marginal distribution $p(\mathbf{x}_n|\mathbf{y}_{0:n},\Theta)$ by generating B particles: $\{(\mathbf{x}_n^{(b)}, J_n^{(b)}), w_n^{(b)}\}_{b=1}^{B}$ for each time $n \in \{0, ..., N\}$ where vectors of $\mathbf{x}_n$ are hypothetical values for the latent state variables, J_n represents the switching process for the paused versus unpaused state, and w_n is a weight generated according to a likelihood of $\mathbf{x}_n$ where $\sum_{b=1}^{B} w_n^{(b)} = 1$ for all $n \in \{0, ..., N\}$. Using (3.2) and the particles $\{(\mathbf{x}_n^{(b)}, J_n^{(b)}), w_n^{(b)}\}_{b=1}^{B}$ generated stochastically using the algorithm, whose description will follow, an approximate distribution of $p(\mathbf{x}_n|\mathbf{y}_{0:n},\Theta)$ can be calculated from a particle bootstrap filter, and we can estimate the integral in Eq (3.1) as

$$\begin{aligned} Q(\Theta|\Theta^{(h)}) \approx \ln[p(\mathbf{x}_0)] &+ \sum_{b=1}^{B}\sum_{n=1}^{N}\sum_{i,j=0}^{1} \ln(\gamma_{ij}) I_{\{J_n^{(b)}=i|J_{n-1}^{(b)}=j\}} w_n^{(b)} + \sum_{b=1}^{B}\sum_{n=0}^{N} \ln[p(\mathbf{y}_n|\mathbf{x}_n^{(b)},\theta_{\mathbf{Y}})] w_n^{(b)} \\ &+ \sum_{b=1}^{B}\sum_{n=1}^{N} \ln[p(\mathbf{x}_n^{(b)}|\mathbf{x}_{n-1}^{(b)}, J_{n-1}^{(b)},\theta_{\mathbf{X}})] w_n^{(b)}\ . \end{aligned} \tag{3.3}$$

We now begin obtaining the updates to the parameters assuming that the weights can be calculated in the previous iteration, enabling the M-step of the EM algorithm. Beginning with the parameters in the state equations, namely $\Theta_{\mathbf{X}}$, recall that all ϵ terms are assumed to be mutually independently and identically distributed Gaussian random variables; more specifically, we assume $(\epsilon_n^{\parallel}, \epsilon_n^{\perp}, \epsilon_n^{\theta}, \epsilon_n^{\delta}) \sim \mathcal{N}_4(\mathbf{0}_4, \mathbf{I}_4)$, then we have the distribution $\mathbf{X}_n|\mathbf{X}_{n-1} \sim \mathcal{N}_4(\mu_{\mathbf{X_n}|\mathbf{X_{n-1}}}, \Sigma_{\mathbf{X_n}|\mathbf{X_{n-1}}})$, where $\mathbf{X}_n = (M_n^x, M_n^y, \theta_n, \delta_n)'$, and the conditional mean vector and conditional covariance matrix are

$$\mu_{\mathbf{X_n}|\mathbf{X_{n-1}}} = \begin{pmatrix} M_{n-1}^x + \Delta(\mu - \beta|\delta_{n-1}|)\cos(\theta_{n-1})I_{\{J_{n-1}=0\}} \\ M_{n-1}^y + \Delta(\mu - \beta|\delta_{n-1}|)\sin(\theta_{n-1})I_{\{J_{n-1}=0\}} \\ \theta_{n-1} \\ (1-\alpha\Delta)\delta_{n-1} \end{pmatrix},$$

$$\Sigma_{\mathbf{X_n}|\mathbf{X_{n-1}}} = \Delta \begin{bmatrix} (\sigma_{\parallel}^2\cos^2(\theta_{n-1}) + \sigma_{\perp}^2\sin^2(\theta_{n-1})) & \cos(\theta_{n-1})\sin(\theta_{n-1})(\sigma_{\parallel}^2 - \sigma_{\perp}^2) & 0 & 0 \\ \cos(\theta_{n-1})\sin(\theta_{n-1})(\sigma_{\parallel}^2 - \sigma_{\perp}^2) & (\sigma_{\parallel}^2\sin^2(\theta_{n-1}) + \sigma_{\perp}^2\cos^2(\theta_{n-1})) & 0 & 0 \\ 0 & 0 & \sigma_{\theta}^2 & 0 \\ 0 & 0 & 0 & \sigma_{\delta}^2 \end{bmatrix}.$$

Similarly with the observation Eq (2.7), containing $\Theta_{\mathbf{Y}}$, then with the continued assumption that $(\epsilon_n^{U^{\mathrm{x}}}, \epsilon_n^{U^{\mathrm{y}}}, \epsilon_n^{L^{\mathrm{x}}}, \epsilon_n^{L^{\mathrm{y}}}, \epsilon_n^{C^{\mathrm{x}}}, \epsilon_n^{C^{\mathrm{y}}}) \sim \mathcal{N}_6(\mathbf{0}_6, \mathbf{I}_6)$, we have that

$$\mathbf{Y}_n|\mathbf{X}_n, \Theta_{\mathbf{Y}} \sim \mathcal{N}_6(\mu_{\mathbf{Y}_n|\mathbf{X}_n}, \Sigma_{\mathbf{Y}_n|\mathbf{X}_n}),$$

where $\mu_{\mathbf{Y}_n|\mathbf{X}_n} = \mathbf{f}(M_n^x, M_n^y, \theta_n, \delta_n)$ with the function $\mathbf{f}$ defined in (2.7) and the conditional covariance defined as a block matrix, where $\mathbf{I}_k$ is the $k \times k$ identity matrix, as

$$\Sigma_{\mathbf{Y}_n|\mathbf{X}_n} = \begin{bmatrix} \sigma^2\mathbf{I}_4 & \mathbf{0} \\ \mathbf{0} & \sigma_c^2\mathbf{I}_2 \end{bmatrix}.$$

Ultimately by lumping any terms that are either constant or do not depend on any of the parameters in Θ all into a single constant K, the E-step approximate expression is thus

$$\begin{aligned} Q(\Theta|\Theta^{(h)}) \approx\ & K - 2(N+1)\ln(\sigma^2) - (N+1)\ln(\sigma_c^2) \\ & - \frac{1}{2}\sum_{n=0}^{N}\sum_{b=1}^{B}\left\|\Sigma_{\mathbf{Y}_n|\mathbf{X}_n}^{-1/2}\left(\mathbf{y}_n - \mu_{\mathbf{Y}_n|\mathbf{X}_n}\right)\right\|^2 w_n^{(b)} \\ & - \frac{N}{2}\ln(\sigma_{\parallel}^2) - \frac{N}{2}\ln(\sigma_{\perp}^2) - \frac{N}{2}\ln(\sigma_{\theta}^2) - \frac{N}{2}\ln(\sigma_{\delta}^2) \\ & - \frac{1}{2\Delta\sigma_{\parallel}^2}\sum_{n=1}^{N}\sum_{b=1}^{B}\left[\Delta_y^{(b)}\sin(\theta_{n-1}^{(b)}) + \Delta_x^{(b)}\cos(\theta_{n-1}^{(b)}) - \Delta(\mu - \beta|\delta_{n-1}^{(b)}|)I_{\{J_{n-1}=0\}}\right]^2 w_n^{(b)} \\ & - \frac{1}{2\Delta\sigma_{\perp}^2}\sum_{n=1}^{N}\sum_{b=1}^{B}\left[\Delta_y^{(b)}\cos(\theta_{n-1}^{(b)}) - \Delta_x^{(b)}\sin(\theta_{n-1}^{(b)})\right]^2 w_n^{(b)} \\ & - \frac{1}{2\Delta\sigma_{\theta}^2}\sum_{n=1}^{N}\sum_{b=1}^{B}\left(\theta_n^{(b)} - \theta_{n-1}^{(b)}\right)^2 w_n^{(b)} - \frac{1}{2\Delta\sigma_{\delta}^2}\sum_{n=0}^{N}\sum_{b=1}^{B}\left(\delta_n^{(b)} - (1-\alpha\Delta)\delta_{n-1}^{(b)}\right)^2 w_n^{(b)} \\ & + \sum_{n=1}^{N}\sum_{b=1}^{B}\sum_{i,j=0}^{1}\ln(\gamma_{ij})I_{\{J_{n-1}^{(b)}=i, J_n^{(b)}=j\}}w_n^{(b)}, \end{aligned} \tag{3.4}$$

where $\Delta_x^{(b)} = M_n^{x(b)} - M_{n-1}^{x(b)}$ and $\Delta_y^{(b)} = M_n^{y(b)} - M_{n-1}^{y(b)}$. This closed-formed approximation that in (3.4) readily allows the M-step to find the vector Θ that maximizes $Q(\Theta|\Theta^{(h)})$. The formulas for all estimators can be readily obtained and are listed in the appendix.

4. Results

This section presents analysis of two types of data. The first part depicts experiments carried out for simulated time series and the second part applies our model and algorithm to time series analysis resulting from experimental microtubule gliding assay data.

4.1. Synthetic data

In this subsection, we will simulate data from the proposed model and use statistical methods to fit parameters for the synthesized data. The simulations shown in this subsection were all generated using the parameter values (which will be referred as the "true" parameter values in this subsection) as shown in Table 1. Each series contains $N = 501$ observations recorded $\Delta = 0.064$ seconds apart. The total length of the microtubule was taken to be 2.8 μm, the shape of any bend in the microtubule was assumed to be parabolic, and the total particle count of size $B = 10,000$ was used at each time index n.

Table 1. The list of parameter values used to generate the simulated time series.

Parameter	Brief Description	Initial Value
σ^2	Variance component of endpoints of MT	2500 nm^2
σ_c^2	Variance component of centroid of MT	100 nm^2
μ	Speed of MT along substrate	250 nm/sec
$\sigma_{\parallel}^2$	Diffusion coefficient for midpoint in direction of MT movement	2500 nm^2/sec
$\sigma_{\perp}^2$	Diffusion coefficient for midpoint transverse to MT movement	100 nm^2/sec
σ_{θ}^2	Diffusion coefficient for rotation of direction of MT	0.0625 rad^2/sec
σ_{δ}^2	Diffusion coefficient for distance between midpoint and centroid	400 nm^2/sec
α	Spring constant for MT to return to straight segment	0.78125 sec^{-1}
β	Coefficient for linear reduction in speed based on curvature	1.0 sec^{-1}
γ_{01}	Probability of switching MT movement from unpaused to paused	0.005
γ_{10}	Probability of switching MT movement from paused to unpaused	0.025

Two basic experiments have results depicted in Figures 3 and 4. Both experiments simulate 100 series with their true parameters as seen in Table 1, which were selected from simplistic analysis through collaboration with The Hancock Lab headed by Dr. William Hancock. The first of these experiments, associated with Figure 3, uses the set of initial parameter estimates $\Theta^{(0)}$ for the EM algorithm as the same as the true parameters used to simulate these series. The second of these, associated with Figure 4, uses the set of initial parameter estimates that are uniformly distributed around each of the respective true parameter values with a lower bound of 40% and an upper bound of 160% of the true value.

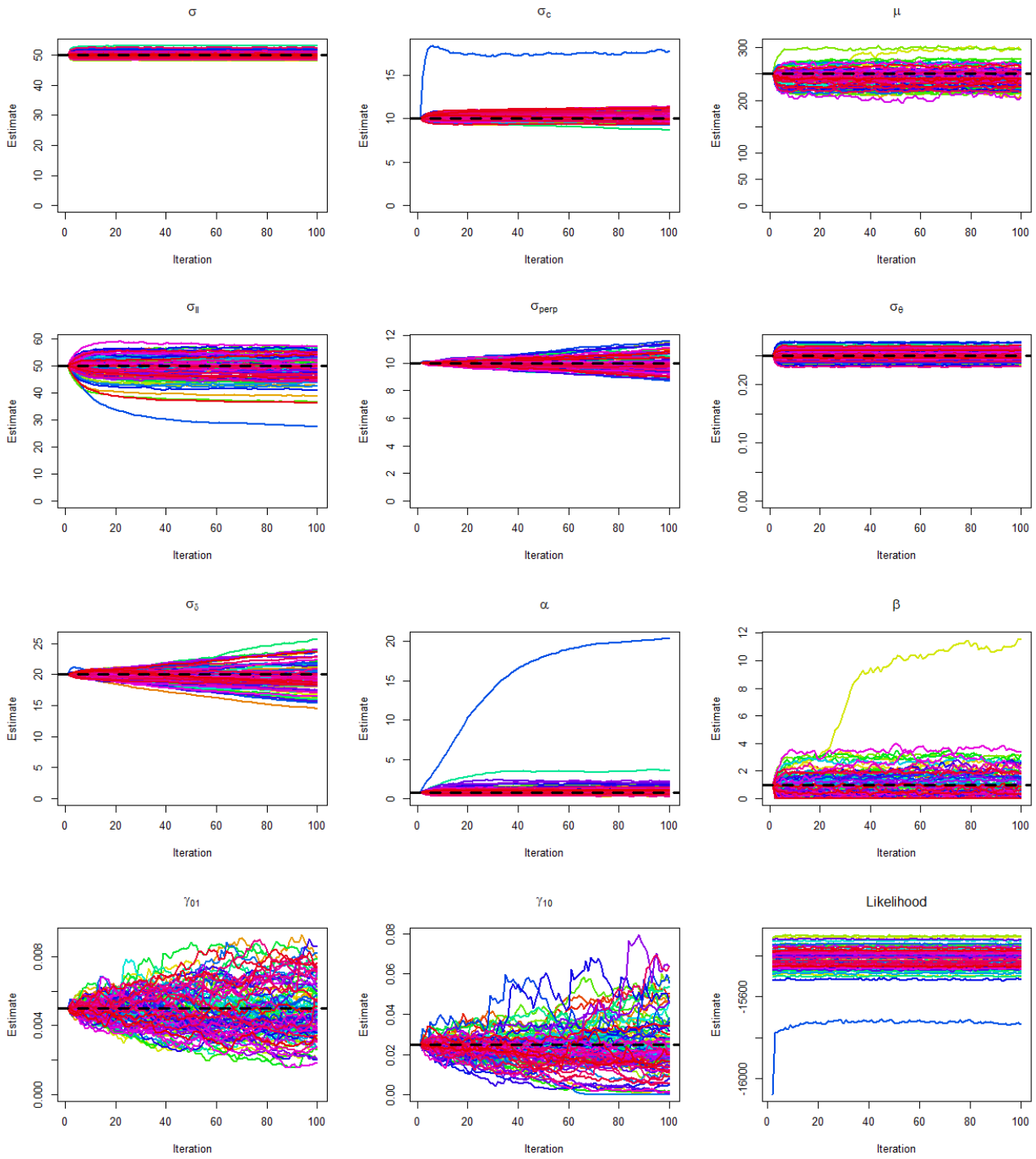


Figure 3. The results of 100 simulations generated under the framework of the full model, each having 100 iterations of the EM algorithm performed. The true values used to simulate each series are shown in the dashed black line. In this experiment, the EM algorithm was provided an initial value for each parameter equal to the true value of the parameter used to generate the simulations. The plot in the lower right corner depicts a stochastic approximation of the likelihood.

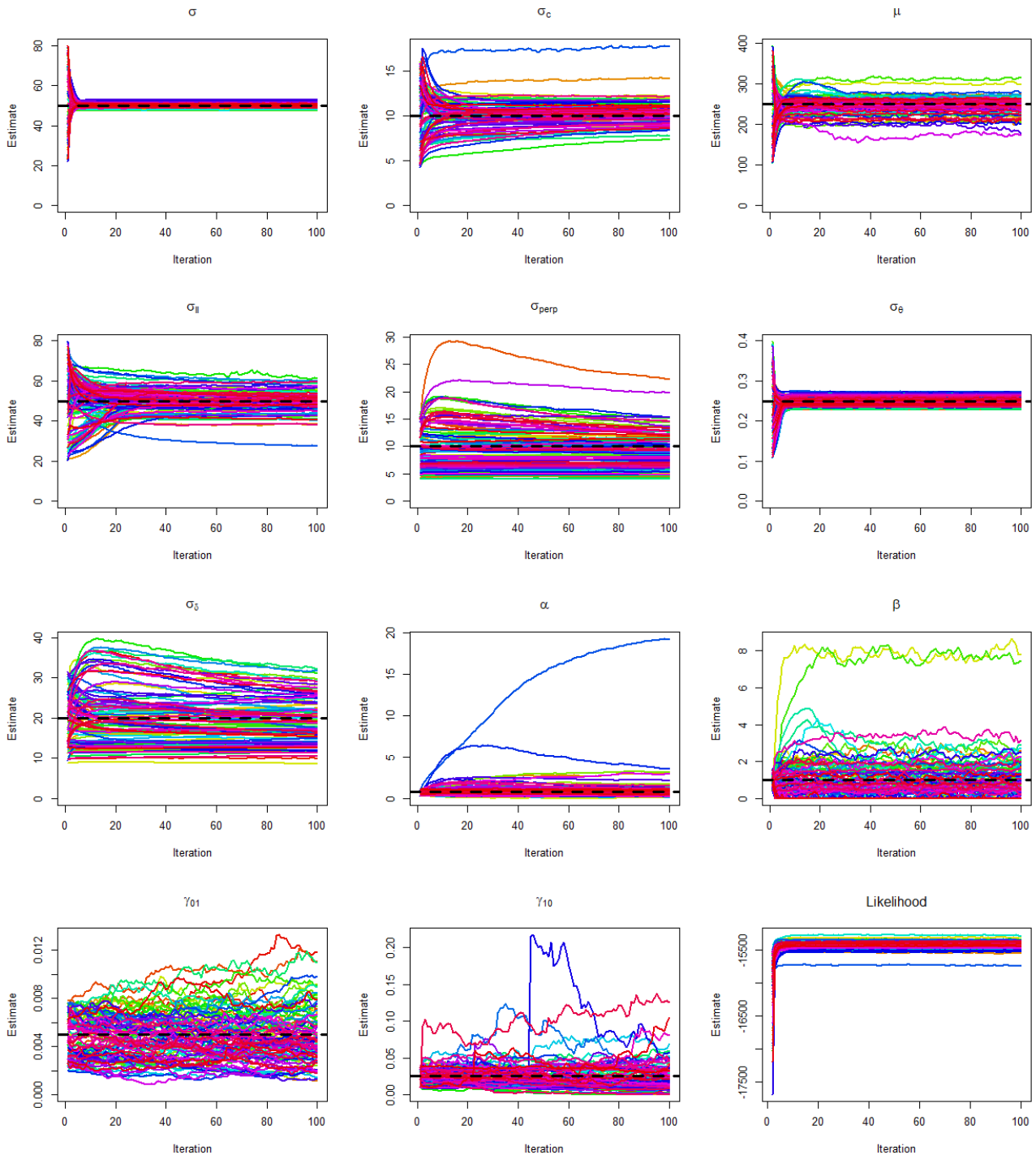


Figure 4. The results of 100 simulations generated under the framework of the full model, each having 100 iterations of the EM algorithm performed. The true values used to simulate each series are shown in the dotted black line. In this experiment, the EM algorithm was provided an initial value for each parameter that was generated from a uniform distributed with a lower bound that was $0.4\theta_0$ and an upper bound of $1.6\theta_0$, where θ_0 is the true value of the parameter used for generating the simulations. The plot in the lower right corner depicts a stochastic approximation of the likelihood.

In either type of simulation, the convergence of the algorithm was generally satisfactory. With a small number of exceptions, the successive parameter estimates stabilized within the 100 iterations shown; some parameter estimates were able to converge within 10 to 20 iterations. The results for σ^2, μ, and σ_θ^2 were not only quick to converge, but the value to which they converged was close to the true parameter value indicating a strong sensitivity our model has to these parameters. Although convergence did not appear to be an issue for parameters such as σ_c^2, $\sigma_\parallel^2$, $\sigma_\perp^2$, and σ_δ^2, unsubstantial changes occurred from their respective initial values across all iterations without any noticeable effect on the approximate likelihood computation. This indicates that our model is somewhat insensitive to the effects of these parameters. The remaining parameters of α, β, γ_{01}, and γ_{10} each showed convergence in most cases within the 100 iterations demonstrated, but with substantial dependency on their respective initial values and a notably large variation for estimates. The conclusion we draw is that our model is insensitive to these parameters. We believe the parameters α and β appeared to be insensitive to our model in part because of the complexity of computing δ_n, which has several layers of noise and dependency on another state variable, θ_n. Additionally, the parameters of γ_{01} and γ_{10} were often difficult to identify due to very rare instances of microtubule pausing when using the initial parameter settings consistent with recommendations in emulating empirical data. Figures 3 and 4 notably depict sequences of parameter estimations that drastically deviate from the other typical paths, which, to the best of our insight, may simply be that conducting optimization in a stochastic environment is likely to produce such outlying results.

We now compare the performance of both versions of the model with one of the simulated series. Figures A1 and A2, in the appendix below, depict the residuals respectively for implementing the full and reduced models where the simulation was generated using the full model. The residuals for the leading point of the simulated microtubule (labeled "Ux" and "Uy" in the figures) and the back point (labeled "Lx" and "Ly" in the figures) depict an adequate fit for the model. However, the residuals for the centroid (labeled "Cx" and "Cy" in Figure A1) indicate dependency using the full model. As for the quality of the fit, the full model yielded a corrected Akaike information criterion (AICc) of 30,671.37 and a Bayesian information criterion (BIC) of 30,717.21. Meanwhile, the reduced version yielded an AICc of 22,581.79 and a BIC of 22,611.08. Thus, these simulations indicate that the modifications to the model to account for curvature do not improve the quality of the parameter estimation.

4.2. Experimentally observed data

The experimental data we will use to demonstrate our methods came from 28 microtubule samples that were polymerized from tubulin in bovine brain where the environment of each experiment kinesin-1 motors from *Drosophilia* (i.e., common fruit flies) adsorbed to glass surfaces that were biotinylated and labeled with green fluorescent proteins (GFP). For more information on their experiments, the reader is referred to [11], who produced the experimental data and were generous in providing it as the basis of this statistical analysis. This paper will exclusively focus on experiments carried out using a glass surface, which was used as the control set of microtubule gliding assay experiments for the study performed as outlined in [11].

One problem encountered in the experimental data was that of missing data. A feature of the EM algorithm is its adaptability for missing observations. Data were recorded at a constant rate of 18.3 frames per second for a difference in time between observations of $\Delta = 0.05451$ seconds. However, there were several occasions where the time between recorded observations was some multiple of Δ

greater than one due to occasional dropped frames. In some uncommon instances, a clear tracking error in the location of the endpoints of the microtubule was present in the data where one or both endpoints were unrealistically far from a proper trajectory for the microtubule during its transit. Such hand-selected instances of an obvious tracking error were treated as missing values within its series.

The only change to the algorithm, apart from what is shown in the appendix, to account for these instances of data considered missing is the following. The particles associated with the state variables $\tilde{\mathbf{x}}_{n+1}^{(b)}$ are updated at each time corresponding to a missing observation according to Eq (2.8), (2.3), and (2.6) and each $J^{(b)}$ is resampled. Conversely, weights are not calculated and bootstrap resampling does not occur. Once the next present observation is reached, the process continues as normal.

The results of running 200 iterations of our stochastic EM algorithm for the full version of the model using the experimental data are depicted in Figure 5 and 200 separate iterations using the reduced version of the model have their results depicted in Figure 6. Many of the same conclusions that were drawn from the previous simulated series can be made with these results. Convergence appeared to have occurred in most cases for all parameters with the exceptions of γ_{01} and γ_{10}. The conclusion for the average speed of a microtubule resulting from the full model was $0.820 \pm 0.041\ \mu m/sec$ at 95% confidence and the reduced model indicated the average speed of $0.791 \pm 0.054\ \mu m/sec$ at 95% confidence.

It is worth identifying that the parameter estimates for σ^2, σ_c^2, μ, $\sigma_\parallel^2$, and σ_θ^2 featured rapid convergence in most cases. Several of the series exhibited early hills in the parameter estimates for σ_c^2 and early valleys in the parameter estimates for $\sigma_\parallel^2$. We will discuss potential reasons that may cause this later, but it is worth identifying specifically that these same series showed the slowest rises in the approximate log-likelihood estimates. This resulted to our belief that the model is sensitive to these parameters.

The remaining estimates $\sigma_\perp^2$, σ_δ^2, α, β, γ_{01}, and γ_{10} did not demonstrate a clear pattern of convergence within the EM iterations performed. However, the resulting approximate likelihood computation appeared to be unaffected. Thus, it appeared that the model is highly insensitive to these parameters, which can be interpreted as having effects that are insignificant. Recall that the parameters σ_δ^2, α, and β are all related to the effect that the curvature of the microtubules has on the movement of the microtubule. The conclusion we drew is that we have not found evidence that curvature is necessary for drawing inferences on microtubule motility in glass surface substrate experiments. This can be corroborated through model comparison: the AICc and BIC suggest a perference for the reduced version of the model for all 28 series (Table A1 depicts all such values).

The parameters γ_{01} and γ_{10} are connected to the cessation or continuation of the movement of the microtubule in both versions of the model. Convergence did not appear to occur in any series regardless of the type of model, and yet the consequence of this had no apparent effect on the likelihood computation. Empirically clear instances of pausing in microtubule movement were either rare or not present in all series, and this is perhaps reflected in this result.

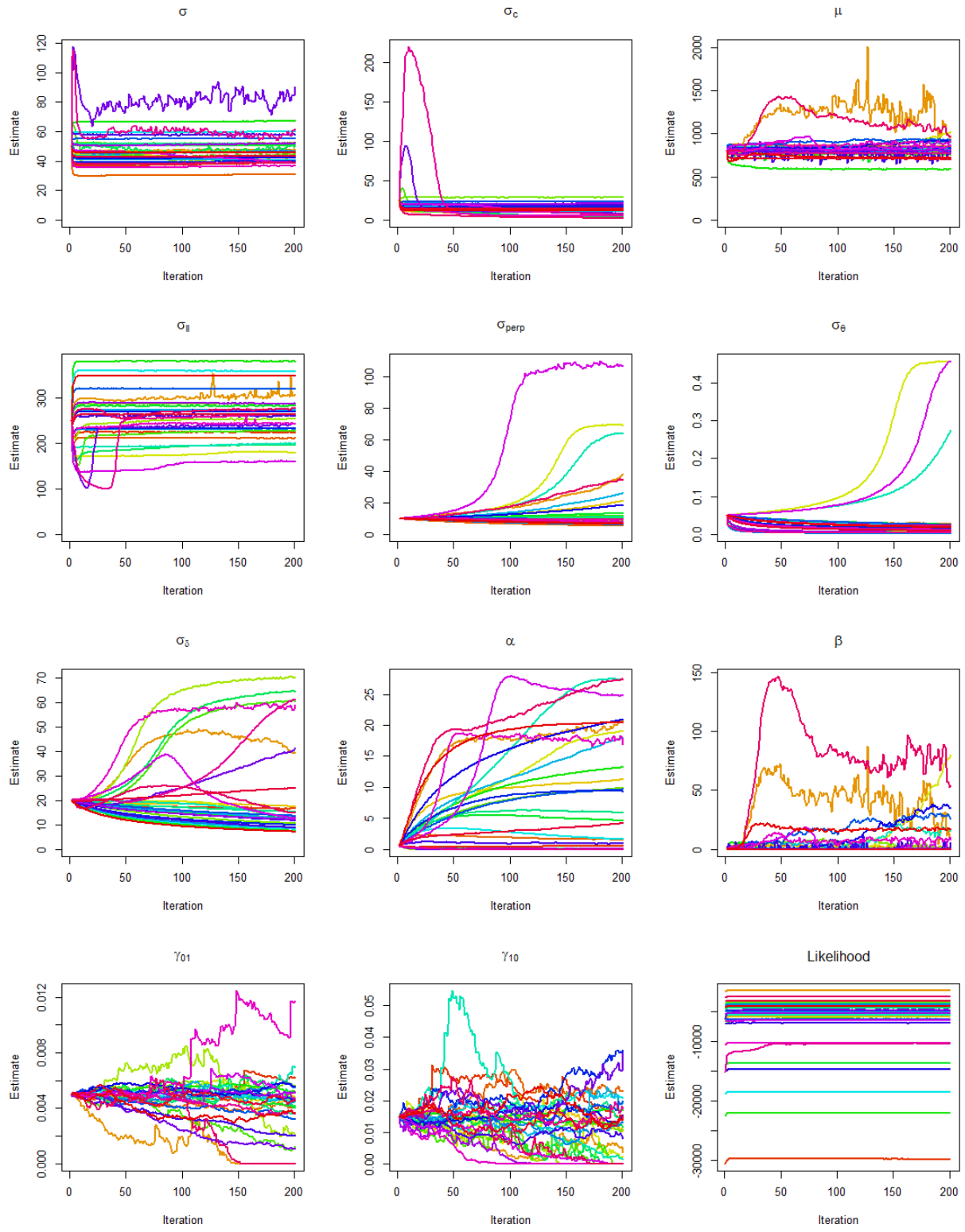


Figure 5. The results of 200 iterations of the stochastic EM algorithm for the 28 series of experimental data across the 11 parameters using the full version of the model as well as a stochastic estimate of the log-likelihood. Matching colors across each of the graphs designate the same series.

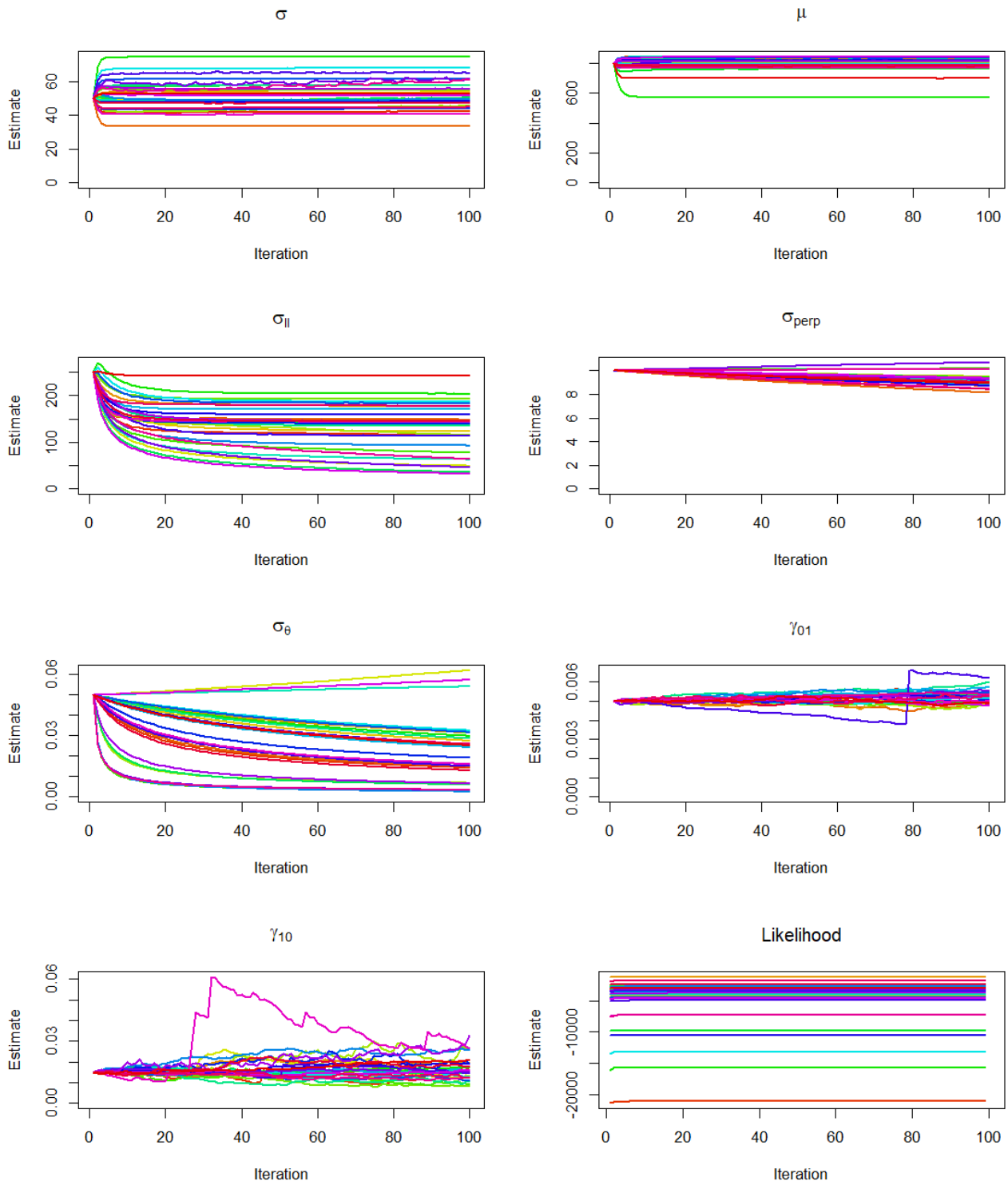


Figure 6. The results of 200 iterations of the stochastic EM algorithm for the 28 series of experimental data across the seven parameters remaining after removing any aspect related to microtubule bending to form the reduced version of the model. The stochastic estimate of the log-likelihood is also included. Matching colors across each of the graphs designate the same series.

We now take time to identify some interesting observations within this set of parameter estimations. We previously mentioned several series with hills or valleys in the estimates for σ_c^2 and $\sigma_\parallel^2$, which are all series in which the centroids did not behave in a manner consistent with the spring mechanism proposed in our model, but instead appeared to bend further outward through time. Such cases also yielded some interesting commonalities, such as less stable estimation in σ in both models, large values for σ_δ, and residuals that better fit an order-1 autoregressive model (particularly with the centroid).

The shortest of all the series produced unstable estimates throughout all iterations for most of the parameter estimates; however, these series can be easily identified by the erratic parameter estimates for both μ and β in the plots corresponding to the full version. Note that the parameter estimates either converge or exhibit stability in the reduced version of the model for these same series.

The three series for which the estimates for σ_θ^2 increase in either version of the model and appear to not converge in the given iterations correspond to the series for which the microtubule length, λ, is the shortest, leading us to infer that the length of the microtubule impacts its frequency for changing direction. Indeed, we found a significant linear correlation between the reciprocal of the final estimate for σ_θ^2 and λ from each series (p-value $\approx 1.15 \times 10^{-14}$). These series also commonly did not find convergence in the parameter estimates for σ_δ^2 and α and includes the series where $\sigma_\perp^2$ rises rapidly for the full model.

In conducting residual analysis for the results, excluding the series mentioned above with notable issues, most of the results yielded residuals that behave in a manner favorable to the model. One such series has been highlighted in the series of plots, Figures A3 through A9 are given in the appendix of this paper. The models assumes a normal distribution for these residuals, and most of the series yielded satisfying corroboration to this assumption. We looked for trends in the residuals and occasionally found that an order-1 autoregressive model was more adequate to explain the relationship for individual residual sets over a more desirable white-noise model; this was particularly the case with series with a higher observation count, say 500 or more observations. When we compared the standardized residuals of the abscissa for the leading and back point of a microtubule, or similarly for the ordinate, using the full version of the model, a significant negative correlation often emerged; however, the same series using the reduced version of the model would often retain a negative correlation but with a notable drop in the strength of its correlation.

5. Conclusions

In this work, we tested two versions of a model framework using particle filtering, with its Bayesian approach involving prior distributions, and a stochastic EM algorithm, involving a frequentist approach via maximum likelihood estimation. Such methodology was not previously carried out for microtubule gliding assay experiments. Whether the result of simulated series or experiment data, some important insight was gained as to how useful a parameter is to understanding the behavior of a microtubule in a gliding assay type experiment. The most notable and significant conclusion was an approximate average speed for these microtubules of 0.8 $\mu m/sec$, corroborating the similar result in [8]. There appears to be little to no improvement in forming inferences in microtubule gliding assay experiments as a result of the factors considered in this paper that were an extension of the model adopted from [12]. We likely have too few clearly observable instances of microtubule pausing its transit, which may be the cause of the model displaying sensitivity to any parameters attempting to explain the microtubule

transitioning from an unpaused state of movement. Additionally, we found no evidence that curvature applied to a microtubule significantly reduced its speed along a glass substrate. This might indicate that lateral forces imposed on kinesin motors adsorbed to the glass substrate do not, to any significant extent, impact the attachment or detachment of the motor to the microtubule.

Improvements to the model may be of interest for future work on the topic. In particular, our approach was to focus on fitting each microtubule path individually within a state-space model, which may in part be responsible for some of the parameters, such as α (the spring constant reflecting the microtubule returning to a straight segment) and β (a coefficient reflecting the loss in speed as a result of any curvature of the microtubule). Our approach incurred some lengthy computational time requiring up to approximately two weeks to complete 100 iterations of the stochastic EM algorithm for longer microtubule paths. However, it is possible that adopting a nonlinear mixed-effects model could improve identifiability of these parameters by allowing parameters to vary from one microtubule to the next and use all of the observed microtubule paths to then jointly fit all (or multiple) microtubule paths. Doing so would increase computation time, though it is an interesting possibility for future work on this topic.

Use of AI tools declaration

The authors declare they have not used Artificial Intelligence (AI) tools in the creation of this article.

Acknowledgments

John Fricks received partial financial support from the French government in the framework of the France 2030 program IdEx Université de Bordeaux. John Stockton and John Fricks were partially supported by US National Institutes of Health grant R01GM122082.

Conflict of interest

The authors declare there is no conflict of interest.

References

1. R. D. Vale, T. S. Reese, M. P. Sheetz, Identification of a novel force-generating protein, kinesin, involved in microtubule-based motility, *Cell*, **42** (1985), 39–50. https://doi.org/10.1016/S0092-8674(85)80099-4
2. J. Howard, A. J. Hudspeth, R. D. Vale, Movement of microtubules by single kinesin molecules, *Nature*, **342** (1989), 154–158. https://doi.org/10.1038/342154a0
3. C. V. Sindelar, K. H. Downing. The beginning of kinesin's force-generating cycle visualized at 9-Å resolution, *J. Cell Biol.*, **177** (2007), 377–385. https://doi.org/10.1083/jcb.200612090
4. N. Hirokawa, K. K. Pfister, H. Yorifuji, M. C. Wagner, S. T. Brady, G. S. Bloom, Submolecular domains of bovine brain kinesin identified by electron microscopy and monoclonal antibody decoration, *Cell*, **56** (1989), 867–878. https://doi.org/10.1016/0092-8674(89)90691-0
5. A. Yildiz, M. Tomishige, R. D. Vale, P. R. Selvin, Kinesin walks hand-over-hand, *Science*, **303** (2004), 676–678. https://doi.org/10.1126/science.1093753

6. S. E. Rice, A. W. Lin, D. Safer, C. L. Hart, N. I. Naber, B. Carragher, et al., A structural change in the kinesin motor protein that drives motility, *Nature*, **402** (1999), 778–784. https://doi.org/10.1038/45483
7. S. L. Rogers, J. M. Scholey, Motility assays for microtubule motor proteins, *Encycl. Life Sci.*, **2004** (2004). https://doi.org/10.1038/npg.els.0002621
8. W. O. Hancock, J. Howard, Processivity of the motor protein kinesin requires two heads, *J. Cell Biol.*, **140** (1998), 1395–1405. https://doi.org/10.1083/jcb.140.6.1395
9. G. Arpağ, S. Shastry, W. O. Hancock, E. Tüzel, Transport by populations of fast and slow kinesins uncovers novel family-dependent motor characteristics important for in vivo function, *Biophys. J.*, **107** (2014), 1896–1904. https://doi.org/10.1016/j.bpj.2014.09.009
10. R. Grover, J. Fischer, F. W. Schwarz, W. J. Walter, P. Schwille, S. Diez, Transport efficiency of membrane-anchored kinesin-1 motors depends on motor density and diffusivity, *Proc. Natl. Acad. Sci.*, **113** (2016), E7185–E7193. https://doi.org/10.1073/pnas.1611398113
11. R. Jiang, S. Vandal, S. Park, S. Majd, E. Tüzel, W. O. Hancock, Microtubule binding kinetics of membrane-bound kinesin-1 predicts high motor copy numbers on intracellular cargo, *Proc. Natl. Acad. Sci. U.S.A.*, **116** (2019), 26564–26570. https://doi.org/10.1073/pnas.1916204116
12. F. Gibbons, J. Chauwin, M. Despósito, J. V. José, A dynamical model of kinesin-microtubule motility assays, *Biophys. J.*, **80** (2001), 2515–2526. https://doi.org/10.1016/S0006-3495(01)76223-6
13. A. Doucet, N. de Freitas, N. Gordon, An introduction to sequential monte carlo methods, in *Sequential Monte Carlo Methods in Practice*, Springer, (2001), 3–14. https://doi.org/10.1007/978-1-4757-3437-9_1

Appendix

Below are the maximum likelihood estimators mentioned at the conclusion of the section describing how the particle filter and EM algorithm are implemented into the study of the model (combining Eqs (2.3), (2.6), and (2.8) as the state equations, and (2.7) as the observation equations):

$$\hat{\sigma}^{2(h+1)} = \frac{1}{4(N+1)} \sum_{n=0}^{N} \sum_{b=1}^{B} \left\| diag(1,1,1,1,0,0)\left(\mathbf{y}_n - \mathbf{f}(\mathbf{x}_n^{(b)})\right)\right\|^2 w_n^{(b)} ,$$

$$\hat{\sigma}_c^{2(h+1)} = \frac{1}{2(N+1)} \sum_{n=0}^{N} \sum_{b=1}^{B} \left\| diag(0,0,0,0,1,1)\left(\mathbf{y}_n - \mathbf{f}(\mathbf{x}_n^{(b)})\right)\right\|^2 w_n^{(b)} ,$$

where $\mathbf{f}(\cdot)$ is defined in Eq (2.7) above and $diag(\cdot)$ refers to a diagonal matrix with the given vector as its elements on the main diagonal. As for the maximum likelihood estimators for the state equations, the computational formulas are the following:

$$\hat{\mu}^{(h+1)} = \frac{\kappa\phi - \nu\tau}{\Delta(\phi^2 - \psi\tau)},$$

$$\hat{\beta}^{(h+1)} = \frac{\kappa\psi - \nu\phi}{\Delta(\phi^2 - \psi\tau)},$$

$$\hat{\sigma}_{\parallel}^{2(h+1)} = \frac{1}{N\Delta}\sum_{n=1}^{N}\sum_{b=1}^{B}\left((M_n^{y(b)} - M_{n-1}^{y(b)})\sin(\theta_{n-1}^{(b)}) + (M_n^{x(b)} - M_{n-1}^{x(b)})\cos(\theta_{n-1}^{(b)})\right)^2 w_n^{(b)}$$
$$- \frac{2}{N}\nu\hat{\mu}^{(h+1)} + \frac{2}{N}\kappa\hat{\beta}^{(h+1)} + \frac{\Delta}{N}\psi(\hat{\mu}^{(h+1)})^2 - \frac{2\Delta}{N}\phi\hat{\mu}^{(h+1)}\hat{\beta}^{(h+1)} + \frac{\Delta}{N}\tau(\hat{\beta}^{(h+1)})^2,$$

$$\hat{\sigma}_{\perp}^{2(h+1)} = \frac{1}{N\Delta}\sum_{n=1}^{N}\sum_{b=1}^{B}\left((M_n^{y(b)} - M_{n-1}^{y(b)})\cos(\theta_{n-1}^{(b)}) - (M_n^{x(b)} - M_{n-1}^{x(b)})\sin(\theta_{n-1}^{(b)})\right)^2 w_n^{(b)},$$

$$\hat{\sigma}_{\theta}^{2(h+1)} = \frac{1}{N\Delta}\sum_{n=1}^{N}\sum_{b=1}^{B}\left(\theta_n^{(b)} - \theta_{n-1}^{(b)}\right)^2 w_n^{(b)},$$

$$\hat{\alpha}^{(h+1)} = \frac{1}{\Delta}\left[1 - \frac{\sum_{n=1}^{N}\sum_{b=1}^{B}\delta_{n-1}^{(b)}\delta_n^{(b)}w_n^{(b)}}{\sum_{n=1}^{N}\sum_{b=1}^{B}(\delta_{n-1}^{(b)})^2 w_n^{(b)}}\right],$$

$$\hat{\sigma}_{\delta}^{2(h+1)} = \frac{1}{N\Delta}\sum_{n=1}^{N}\sum_{b=1}^{B}\left[\delta_n^{(b)} - (1-\hat{\alpha}^{(h+1)})\delta_{n-1}^{(b)}\right]^2 w_n^{(b)},$$

$$\hat{\gamma}_{00}^{(h+1)} = 1 - \hat{\gamma}_{01}^{(h+1)} = \frac{\sum_{n=1}^{N}\sum_{b=1}^{B} I_{\{J_{n-1}^{(b)}=0, J_n^{(b)}=0\}} w_n^{(b)}}{\sum_{n=1}^{N}\sum_{b=1}^{B} I_{\{J_{n-1}^{(b)}=0\}} w_n^{(b)}},$$

$$\hat{\gamma}_{10}^{(h+1)} = 1 - \hat{\gamma}_{11}^{(h+1)} = \frac{\sum_{n=1}^{N}\sum_{b=1}^{B} I_{\{J_{n-1}^{(b)}=1, J_n^{(b)}=0\}} w_n^{(b)}}{\sum_{n=1}^{N}\sum_{b=1}^{B} I_{\{J_{n-1}^{(b)}=1\}} w_n^{(b)}},$$

where:

$$\kappa \equiv \sum_{n=1}^{N}\sum_{b=1}^{B}\left[(M_n^{y(b)} - M_{n-1}^{y(b)})\sin(\theta_{n-1}^{(b)}) + (M_n^{x(b)} - M_{n-1}^{x(b)})\cos(\theta_{n-1}^{(b)})\right]\left|\delta_{n-1}^{(b)}\right| I_{\{J_{n-1}^{(b)}=0\}} w_n^{(b)},$$

$$\nu \equiv \sum_{n=1}^{N}\sum_{b=1}^{B}\left[(M_n^{y(b)} - M_{n-1}^{y(b)})\sin(\theta_{n-1}^{(b)}) + (M_n^{x(b)} - M_{n-1}^{x(b)})\cos(\theta_{n-1}^{(b)})\right] I_{\{J_{n-1}^{(b)}=0\}} w_n^{(b)},$$

$$\psi \equiv \sum_{n=1}^{N}\sum_{b=1}^{B} I_{\{J_{n-1}^{(b)}=0\}} w_n^{(b)},$$

$$\phi \equiv \sum_{n=1}^{N}\sum_{b=1}^{B}\left|\delta_{n-1}^{(b)}\right| I_{\{J_{n-1}^{(b)}=0\}} w_n^{(b)},$$

$$\tau \equiv \sum_{n=1}^{N}\sum_{b=1}^{B}(\delta_{n-1}^{(b)})^2 I_{\{J_{n-1}^{(b)}=0\}} w_n^{(b)}.$$

The following minipage explains the stochastic EM algorithm that was implement for the work in Section 3. Note that the choices for the variances of the prior distributions for θ_0 and δ_0 in the initialization step were arbitrary.

Particle Bootstrap Filter and EM Algorithm [13]

For $h = 1, ..., H$ iterations of the EM algorithm, set $\Theta = \Theta^{(h-1)}$ (the previous iteration). Note that $\Theta_{\mathbf{X}} = \Theta_{\mathbf{X}}^{(h-1)}$ and $\Theta_{\mathbf{Y}} = \Theta_{\mathbf{Y}}^{(h-1)}$ whenever relevant.

Step 1: Initialization

- Center the data such that the midpoint of the first endpoints at index $n = 0$ to (0,0).
- Set $M_0^{x,(b)} = 0$ and $M_0^{y,(b)} = 0$ for all $b = 1, ..., B$.
- Sample $\theta_0^{(b)} \sim N(\theta_0, (\pi/12)^2)$ i.i.d. for each b where θ_0 is the central angle formed by the line segment with the initial point at (L_0^x, L_0^y) and terminal point at (U_0^x, U_0^y).
- Compute δ_0 as the Euclidean distance between (0,0) and the (C_0^x, C_0^y), then assign a "-" or "+" sign depending on whether the microtubule bends left or right, respectively. Then, sample $\delta_0^{(b)} \sim N(\delta_0, (\delta_0/12)^2)$ i.i.d.
- Generate $J_0^{(b)} \sim Bern(p_0)$ i.i.d. where $p_0 = \gamma_{01}/(\gamma_{01} + \gamma_{10})$.
- Set $\tilde{\mathbf{x}}_0^{(b)} = (M_0^{x,(b)}, M_0^{y,(b)}, \theta_0^{(b)}, \delta_0^{(b)})$.
- Evaluate the importance weights $\tilde{w}_0^{(b)} = p(\mathbf{y}_0|\tilde{\mathbf{x}}_0^{(b)}, \Theta_{\mathbf{Y}}^{(h-1)})$.
- For $b = 1, ..., B$, normalize the weights $w_n^{(b)} = \tilde{w}_n^{(b)} / \sum_{b=1}^{B} \tilde{w}_n^{(b)}$.
- Using these weights, update sum expressions in Eq (3.4) involving parameter estimates associated with $\Theta_{\mathbf{Y}}^{(h)}$.
- Set $n = 1$.

Step 2: Importance Sampling

- For $b = 1, ..., B$, sample $\tilde{\mathbf{x}}_n^{(b)} \sim p(\mathbf{x}_n|\mathbf{x}_{n-1}^{(b)}, J_{n-1}^{(b)}, \Theta_{\mathbf{X}}^{(h-1)})$.
- If $J_{n-1}^{(b)} = 0$ (unpaused), sample $J_n^{(b)} \sim Bern(\gamma_{01})$. Else if $J_{n-1}^{(b)} = 1$ (paused), sample $J_n^{(b)} \sim Bern(1 - \gamma_{10})$.
- For $b = 1, ..., B$, evaluate the importance weights $\tilde{w}_n^{(b)} = p(\mathbf{y}_n|\tilde{\mathbf{x}}_n^{(b)}, \Theta_{\mathbf{Y}}^{(h-1)})$.
- For $b = 1, ..., B$, normalize the weights $w_n^{(b)} = \tilde{w}_n^{(b)} / \sum_{b=1}^{B} \tilde{w}_n^{(b)}$.

Step 3: Selection

- Using the weights $w_n^{(b)}$ from step 2, update sum expressions in Eq (3.4) for the current time t toward computing $\theta^{(h)}$.
- Resample with replacement B particles from $\{\tilde{\mathbf{x}}_n^{(b)}, J_n^{(b)}\}_{b=1}^{B}$, using the weights $w_n^{(b)}$ from step 2. Call this resample $\{\mathbf{x}_n^{(b)}, J_n^{(b)}\}_{b=1}^{B}$.
- Set n to $(n + 1)$ and repeat step 2 while $n \leq N$.

Step 4: Finalize EM Estimates

- Complete calculations necessary to complete Eq (3.4).

Below are the residuals for one of the simulated series. The same series was generated assuming the full model is the true model, and the plots below show the result of parameter estimation under the full model (Figure A1) and also run under the [misspecified] reduced model (Figure A2).

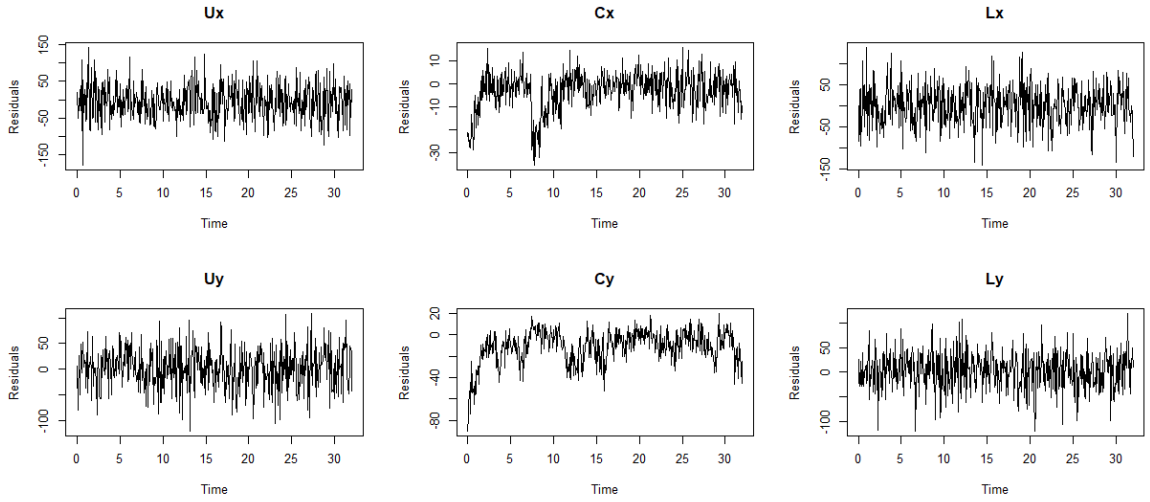


Figure A1. For a series simulated as the full model, this plot depicts the residuals from using the full model as the method of parameter estimation.

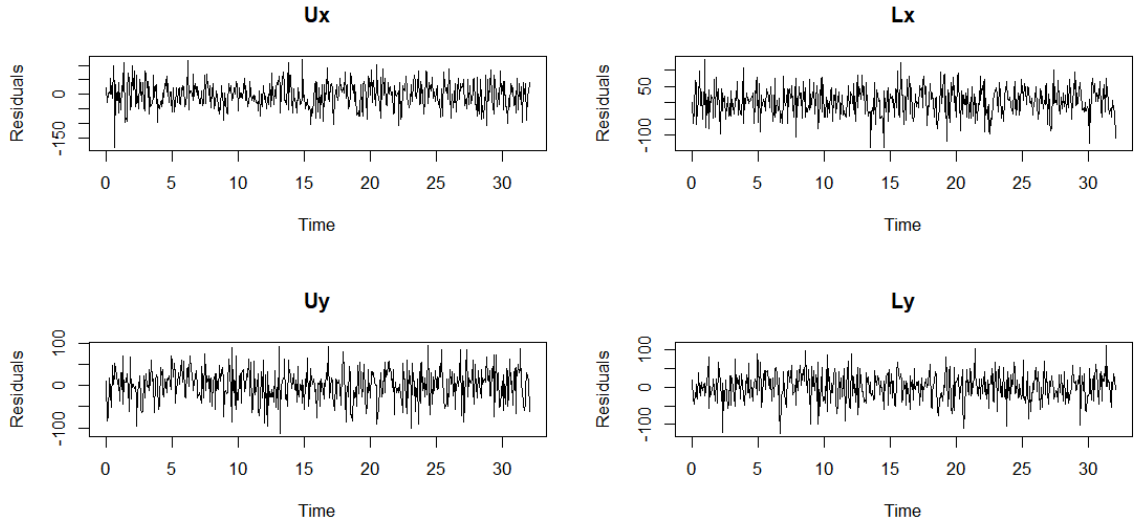


Figure A2. For a series simulated as the full model, this plot depicts the residuals from using the reduced model as the method of parameter estimation.

The following sequence of graphs depicts residual analysis for the same series of experimental data between the full and reduced versions of the model. Accompanying each plot is the p-value for a hypothesis test whose null hypothesis states that standardized residuals are effectively white noise versus an alternative hypothesis stating that an order-1 autoregressive (AR1) model is an adequate fit for its respective set of standardized residuals using the `sarima` package in R. Vertical dashed red lines correspond to time indices for a missing value in the series.

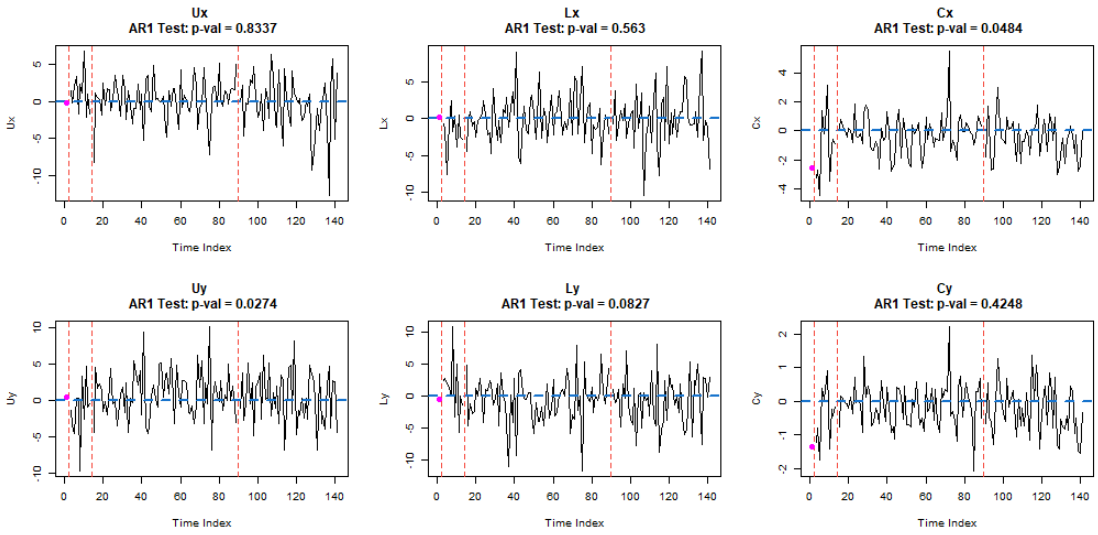


Figure A3. The standardized residuals for each of the six variables considered in the observation equations for the full version of the model.

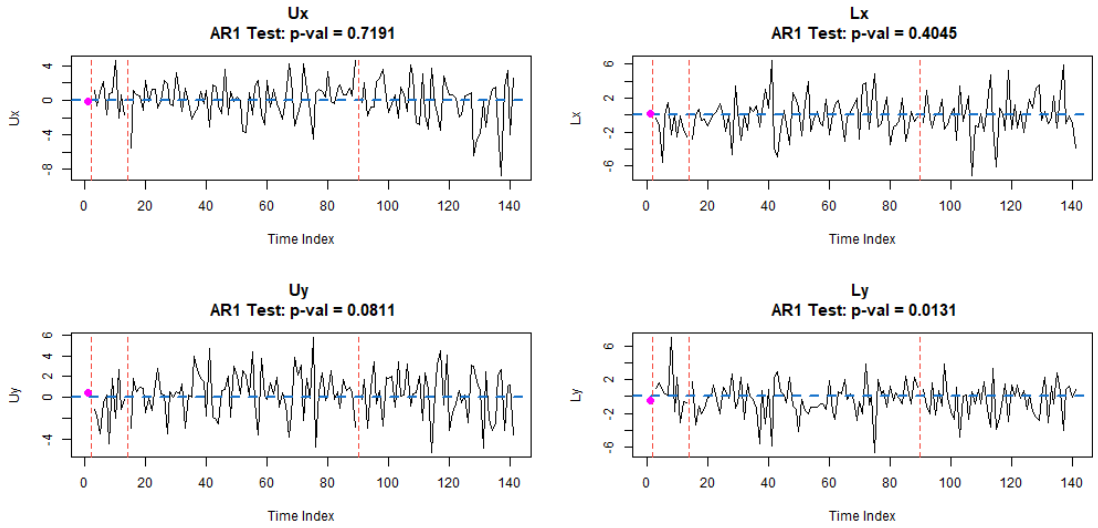


Figure A4. The standardized residuals for each of the four variables considered in the observation equations for the reduced version of the model.

Below are partial autocorrelation function (PACF) plots depicting the partial autocorrelation of the residuals up to a lag of 30 for the same series of experimental data between the full and reduced versions of the model. The red horizontal dashed lines represent the threshold for considering an autoregressive (AR) model of the lag represented on the abscissa to be an appropriate fit (over essentially white noise) at 95% confidence. Because there does not exist any consistent pattern with which partial autocorrelation values exceed the confidence bounds between any of the variables within the full version of the model, this can be interpreted that the residuals may effectively be white noise for this series. The same may be interpreted for the reduced version of the model.

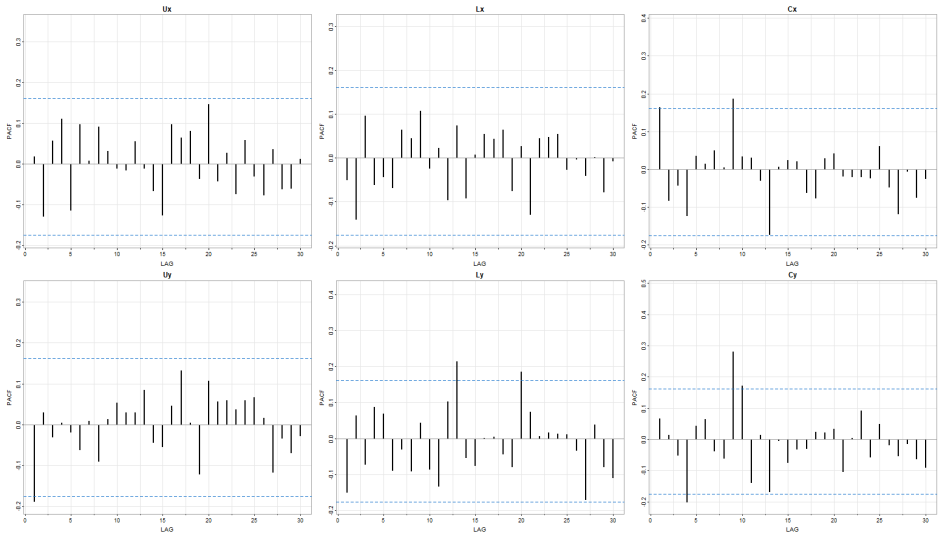


Figure A5. PACF plots for each of the six variables considered in the observation equations for the full version of the model.

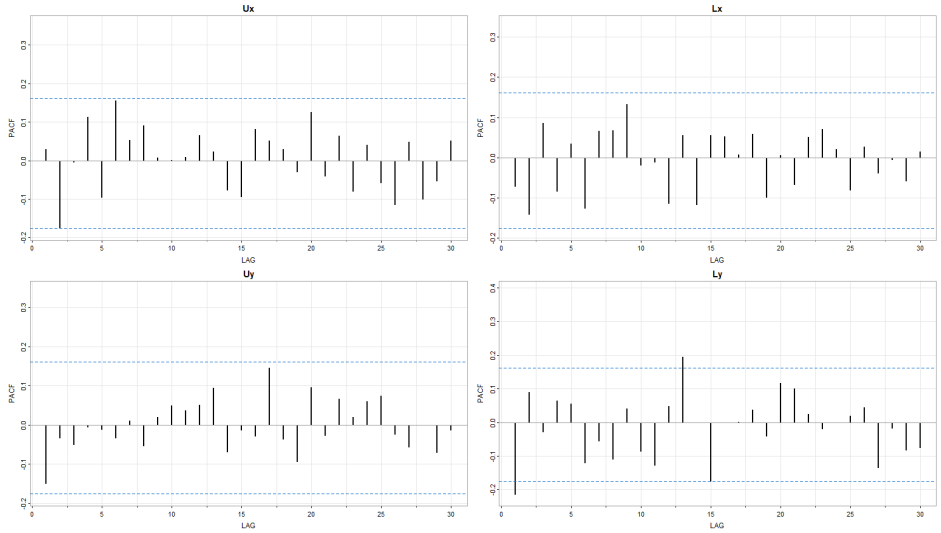


Figure A6. PACF plots for each of the four variables considered in the observation equations for the reduced version of the model.

The plots below are a collection of comparisons between the standardized residuals among the observations from the full version of the model. The top-left plot depicts the relationship between the standardized residuals for the x- and y-coordinates for the leading point of the microtubule. The top-right plot depicts the relationship between those of the x- and y-coordinates for the back point of the microtubule. The bottom-left plot depicts the relationship between the x-coordinates of both the leading and back point of the microtubule. Finally, the bottom-right plot depicts that of the y-coordinates for both points. As identified in the main paper, an elliptic shape can very strongly be used to identify these relationships of the residuals in the full model; while this elliptic shape can still be seen in the reduced version of the model, there is a notable improvement toward a more circular shape that would suggest a general independence between the sets of residuals.

The negative correlation displayed in the plots leads to an interesting consideration of employing correlated noise in the observations as a feature of the model. This can be implemented in future work on this topic, though it would complicate the model adding to the total computation time required; however, we do not believe this relationship is the result of observational error but rather to some discrepency between the underlying biological process and our somewhat simplified model.

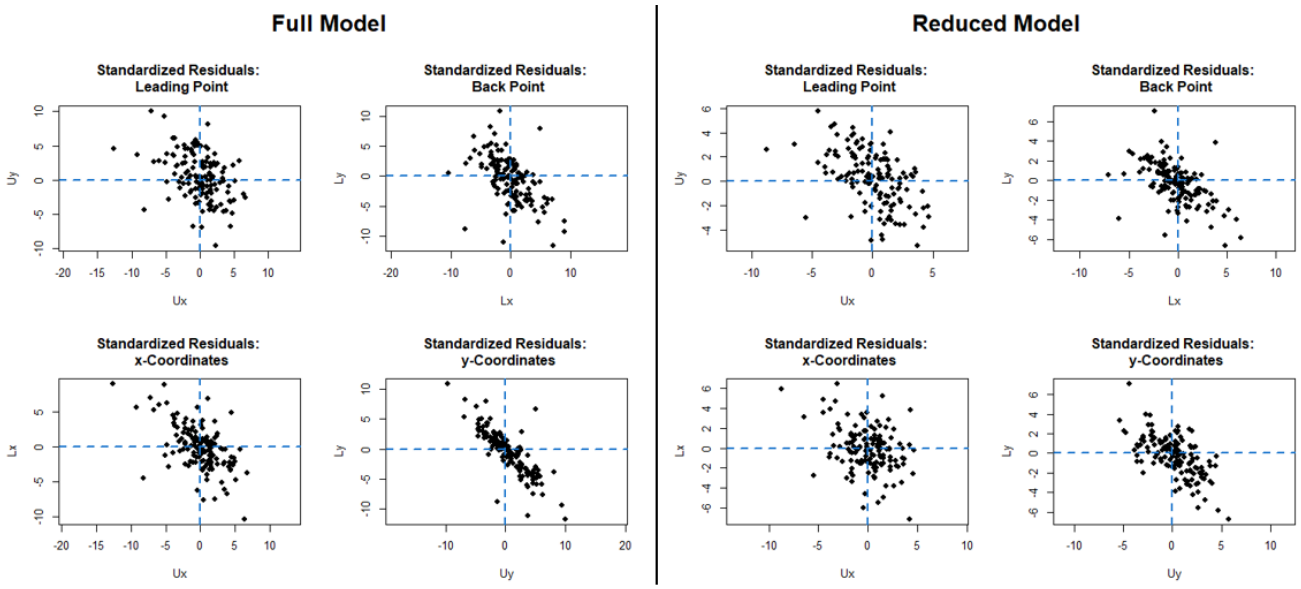


Figure A7. Residual comparison for the full version of the model comprises the 2×2 grid of plots on the left. The 2×2 grid of plots on the right correspond to the results using the reduced version of the model for the same series.

Below are the normal probability plots for the residuals across both versions of the model using the same series. The appropriateness of the normal distribution, as employed by the model, would not be disputed with either version of the model, though the reduced version of the model appears to improve the assumption of the appropriateness of the normal distribution for the residuals of the observation variables. Accompanying each plot is the *p*-value for a Shapiro-Wilk test whose null hypothesis is that a normal distribution is appropriate for its respective set of standardized residuals.

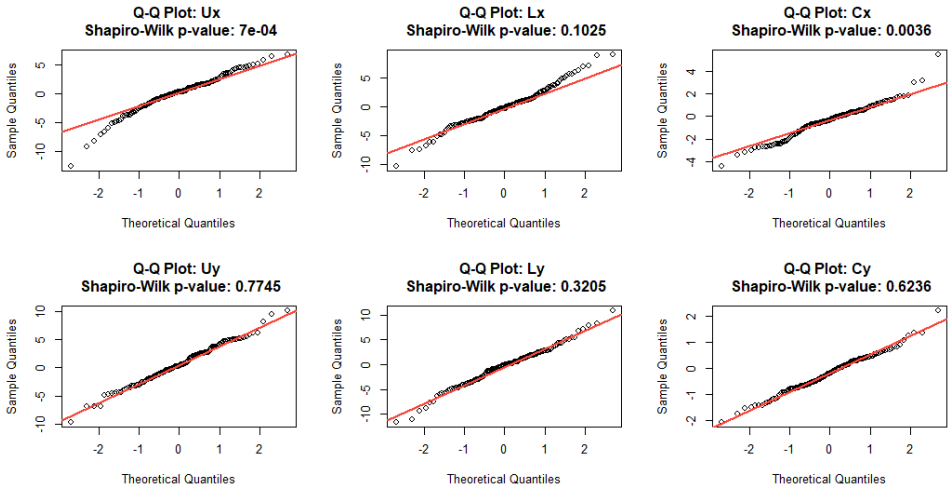


Figure A8. Normal probability plots for the standardized residuals for all six variables in the observation equations in the full version of the model.

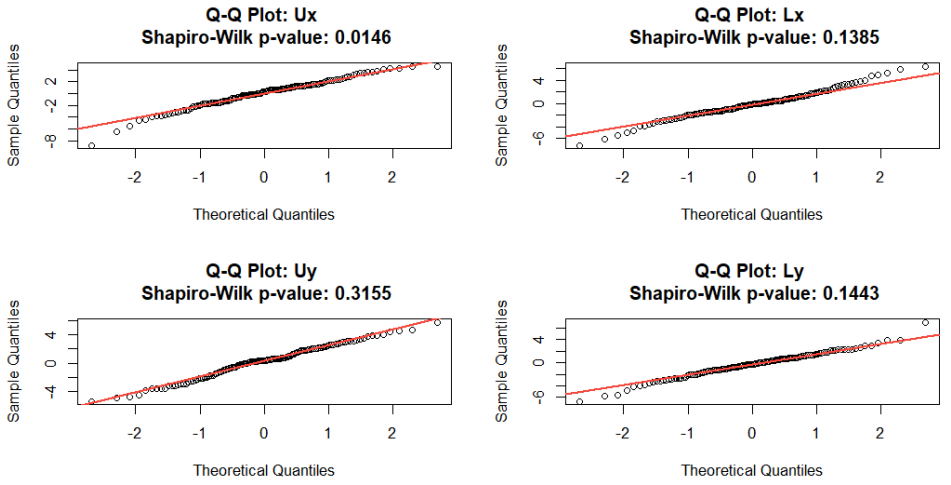


Figure A9. Normal probability plots for the standardized residuals for all four variables in the observation equations in the reduced version of the model.

Table A1. The AICc and BIC values for each series between the full and reduced versions of the model.

Series	AICc, Full	AICc, Reduced	BIC, Full	BIC, Reduced
1	59,632.39	42,402.42	59,686.09	42,436.66
2	8604.90	6153.36	8636.08	6173.59
3	3065.35	2210.43	3079.03	2220.94
4	11,880.35	84,86.50	11,914.71	8508.70
5	12,900.33	9054.55	12,935.76	9077.39
6	6766.35	4772.28	6793.36	4790.09
7	7137.91	5034.02	7165.18	5051.97
8	12,575.71	8973.39	12,610.90	8996.08
9	43,933.49	31,580.44	43,982.70	31,611.84
10	27,375.03	19,467.51	27,419.23	19,495.78
11	7374.12	5170.86	7402.22	5189.30
12	8924.28	6324.18	8954.67	6343.98
13	11,250.15	7936.53	11,283.92	7958.36
14	36,995.96	26,537.51	37,043.39	26,567.79
15	9872.20	7090.06	9904.49	7111.00
16	7650.73	5353.64	7679.28	5372.35
17	12,499.01	8843.64	12,533.51	8865.91
18	9654.06	6870.27	9686.10	6891.06
19	29,358.31	21,038.63	29,403.73	21,067.65
20	13,895.34	9879.71	13931.23	9902.83
21	9632.13	6459.14	9662.80	6479.11
22	10,659.02	7504.29	10,691.69	7525.46
23	12,967.10	9130.21	13,002.58	9153.09
24	20,630.61	14,614.23	20,672.10	14,640.80
25	20,947.58	14,714.33	20,988.43	14,740.51
26	5013.71	3647.63	5036.78	3663.18
27	6518.38	4615.18	6544.87	4632.68
28	8196.55	5948.04	8226.17	5967.38

AIMS Press

© 2026 the Author(s), licensee AIMS Press. This is an open access article distributed under the terms of the Creative Commons Attribution License (https://creativecommons.org/licenses/by/4.0)